Clustering Persistent Scatterer Points Based on a Hybrid Distance Metric

Philipp J. Schneider(✉) and Uwe Soergel

Institute for Photogrammetry, University of Stuttgart, Geschwister-Scholl-Str. 24D, 70174 Stuttgart, Germany
{philipp.schneider,uwe.soergel}@ifp.uni-stuttgart.de

Abstract. Persistent Scatterer Interferometry (PSI) is a powerful radar-based remote sensing technique, able to monitor small displacements by analyzing a temporal stack of coherent synthetic aperture radar images. In an urban environment it is desirable to link the resulting PS points to single buildings and their substructures to allow an integration into building information and monitoring systems. We propose a distance metric that, combined with a dimension reduction, allows a clustering of PS points into local structures which follow a similar deformation behavior over time. Our experiments show that we can extract plausible substructures and their deformation histories on medium sized and large buildings. We present the results of this workflow on a relatively small residential house. Additionally we demonstrate a much larger building with several hundred PS points and dozens of resulting clusters in a web-base platform that allows the investigation of the results in three dimensions.

Keywords: Persistent scatterer interferometry · Clustering · Distance metric

1 Introduction

The remote sensing technique persistent scatterer interferometry (PSI) [8,9] allows monitoring of deformations in large areas such as entire cities. This differential interferometric synthetic aperture radar method is established and well understood. High resulting SAR images lead to millions of persistent scatterer (PS) points in the covered area. The most interesting result of PSI is a deformation time series that describes the points movement, along the satellites line-of-sight, over time with millimeter accuracy. Today the subsequent analysis of deformation processes is often limited to visual inspection of PS point clouds superimposed onto an orthophoto. This is not suitable in order to gain full insight of the 3d distribution and motion patterns of the PS points, especially in an urban environment. In addition, often the deformation time series for each point are condensed to a linear trend. This motion model neglects dynamic characteristics of the PS points and makes it difficult to identify groups of points

C. Bauckhage et al. (Eds.): DAGM GCPR 2021, LNCS 13024, pp. 621–632, 2021.
https://doi.org/10.1007/978-3-030-92659-5_40

that, for example, show similar seasonal deformation behavior. Furthermore, the assignment of PS points to single buildings and later to building substructures is desirable, since this can open the PS-technique for automated per building risk assignment and its integration into long term building information management systems.

In this paper, we propose a clustering approach for PS points based on an initial non-linear dimension reduction and a new distance metric. The resulting clusters show a similar deformation behavior and segment the building in its substructures. The underlying assumption hereby is that PS points on rigid structures show a correlated behavior in their deformation histories. We exploit this fact to cluster them and thereby find groups of points that represent redundant measurements of the underlying deformation process. The spatial distribution of these groups gives an insight into the internal static structure of the building.

Depending on the size of the investigated building, the resulting clusters, their spatial distribution and related time series are complex to visualize. Therefore, we present an exemplary web-based platform which can be used by decision makers, such as civil engineers, to inspect the PS points and the resulting clusters superimposed with a three-dimensional representation of the building.

Previous clustering approaches by [18,20] and [4] have in common that they do not use a correlation based distance metric to describe the similarity between the PS points. [14] show that such PS-clusters can be confirmed by in-situ ground based techniques and introduce a correlation-based distance metric. [15] suggest an initial dimension reduction to counteract problems in high-dimensional clustering.

In the following, we briefly introduce our data set, explain PSI technique and the resulting PS point cloud. We explain the reverse geocoding approach we use to transfer the building labels into the radar geometry in detail. The main focus of this work is the newly proposed distance metric, which combines a correlation based distance with an Euclidean one. Finally, we show results of our approach on an exemplary, relative small building. In the appendix, we provide a link to a web-based three-dimensional presentation of the before shown results, along with another, much larger building.

2 Methods and Data Set

2.1 Synthetic Aperture Radar and Airborne Laser Scanning Data

The here used synthetic aperture radar (SAR) data have been acquired by the German X-Band SAR satellite TerraSAR-X (TSX). The corresponding slant range - azimuth resolution for the "High Resolution Spotlight 300 Mhz acquisition mode" is $0.6\,\mathrm{m} \times 1.1\,\mathrm{m}$ [1]. The 132 images were captured during a 4 years time span (September 2016 to October 2020) with an 11 days repeat cycle. For the interferogram generation a master image in November 2018 was chosen.

We are using sovereign airborne laser scanning (ALS) data (40 Points/m^2, flight altitude: 1000 m) to represent the 3D structure of buildings and to derive a digital surface model (DSM) from this point cloud. The DSM serves as a

reference elevation model for the PSI processing and the label transformation, as well as for the visualization of the PS-clusters on the buildings.

2.2 Study Site

We choose two exemplary buildings to demonstrate our clustering approach. *Building 1* is a relatively small apartment building, which suffers from damage [17] due to an underground tunnel construction. *Building 2* one is a large commercial complex, that was build in 2014. No underground construction is carried out here, but harmless post-construction settlements can be expected here.

2.3 Persistent Scatterer Interferometry

Persistent scatterer interferometry (PSI) is an advanced Differential Interferometric SAR (DInSAR) technique. The main idea of this algorithm is the detection of temporally coherent pixels in a stack of co-registered SAR images. By analyzing the phase history of such pixels in each image of the stack, relative to a master image, the line-of-sight (LOS) movement evolution and a 3d position of this scatterer can be estimated [8,9]. [6] give a good overview over the basics and the capabilities of PSI algorithms. For more detailed insights we highly recommend reading this article.

The results presented here were obtained using ENVI's SARscape software [13] with a temporal coherence threshold of 0.7, which is a good trade of between point quality and density [19].

PSI works well for dense urban areas, since man-made structures especially metal parts located at house façades and roofs act as retro reflectors [16].

Since PSI is analyzing time series of multiple SAR images, the displacement history of each scatterer is one of the results. For every PS point we obtain its relative displacement $d(t)$ as a time series with a measurement for each of the $M = 132$ SAR acquisitions (see Eq. (1)). The accuracy for each measurement can be better than 2 mm [11].

The deformation time series represent the most advanced PSI product and is the base for the later clustering approach. As [10] and [5] have shown, PSI time series, derived from high-resolution SAR data, are able to reveal the annual movements of buildings. They confirm thermal expansion of buildings up to several millimeters in amplitude over the year. We exploit this fact for our clustering, under the assumption that each segment of a building exhibits a characteristic movement behavior.

2.4 Building Footprints and Label Transformation

We use *OpenStreetMap* (OSM) building footprints to assign the extracted PS points to single building entities. We apply a *Reverse Geocoding* approach to transfer the footprints from WGS84 coordinate system to the radar image's range azimuth geometry. The main idea hereby is to utilize an existing pipeline [13]

to geocode two lookup tables (LuTs). The LuTs contain a unique identifier for each range and azimuth cell. After geocoding, these LuTs are used to transfer labels, respectively building footprints, into the master images range-azimuth geometry. This allows precise assignment for each PS point, without the need of the estimated UTM-coordinates. An overview over the entire workflow is given in Fig. 1. Results are shown in Fig. 2. This approach is also suitable to transfer the labels of training data into range-azimuth geometry, e.g. for land classification applications.

The semantic representation of a building as a polygon in OSM is arguably not suitable for a structural analysis. Often, building complexes, as presented in the results in Fig. 5, are divided into several units, even though they are connected and need to be regarded as a single structure. This can be simply overcome by merging the individual components before the analysis. On the other hand, some buildings consist obviously of several independent units but are listed as a single OSM building entity (see Building 2 in Appendix 5). In practice, this does not affect the results too much, since the here proposed distance metric does consider the actual distances of building parts by it-self. The downside is that a larger amount of points has to be considered in the analysis, which has negative effects on the run time.

2.5 Deformation Space

We treat the deformation histories of each PS point as points in a M-dimensional space, with a dimension for each acquisition date. The example in Fig. 3 shows the embedding of such a (exemplary) deformation history for $M = 3$. Each point $d_n \in \mathbb{R}^M$ is defined by the M measurements d:

$$d_n = \left[d_1^n \; d_2^n \; \ldots \; d_{M-1}^n \; d_M^n\right]. \tag{1}$$

In order to have a metric for the Euclidean distance we also use the Cartesian coordinates of the PS points. For the following steps we define the coordinate tuple for each point as:

$$X_n = \left[x_n \; y_n \; z_n\right]. \tag{2}$$

2.6 Distance Metric

We use a combined distance D to describe the similarity of two PS points d_a and d_b in the M-dimensional deformation space. D is composed of the correlation distance D_C which is "1- minus the sample correlation" (see Eq. (4)) and the normalized Euclidean distance D_E between the PS points coordinates X_a and X_b. The normalization is achieved by dividing all distances by the maximum (See Eq. (6)). We combine D_E and D_C as follows:

$$D = \sqrt{D_C^2 + D_E^2 \cdot \lambda}\,. \tag{3}$$

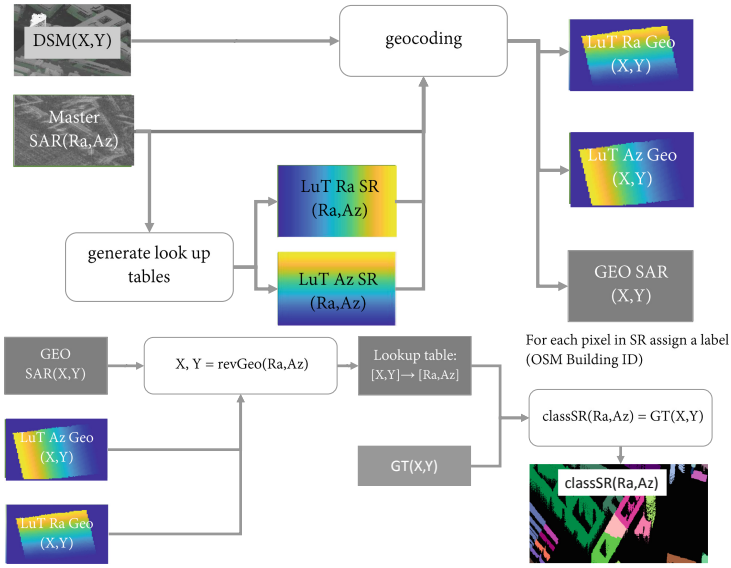

Fig. 1. Workflow for Reverse Geocoding: We generate Lookup tables (LuTs) for Range and Azimuth based on the dimensions and acquisition parameters of the master image. The LuTs are geocoded, using the master image's SAR properties and a precise digital surface model (DSM) derived from the ALS point cloud. The geocoded LuTs allow a mapping of the ground truth (GT) from UTM coordinates to slant-range geometry: $X, Y \rightarrow Ra, Az$, including SAR characteristic distortion properties like foreshortening and layover (Fig. 2).

The weight factor λ allows control over the cluster size. In all our experiments we fix it to $\lambda = 1$.

The correlation distance D_C considers two points (d_a and d_b) as close if their deformation behavior is correlated:

$$D_C = 1 - corr(d_a, d_b) \tag{4}$$

$$= 1 - \frac{(d_a - \overline{d_a})(d_b - \overline{d_b})^T}{\sqrt{(d_a - \overline{d_a})(d_a - \overline{d_a})^T} \cdot \sqrt{(d_b - \overline{d_b})(d_b - \overline{d_b})^T}} \tag{5}$$

where $\overline{d_a} = \frac{1}{M} \sum_m^M d_m^a$
$\overline{d_b} = \frac{1}{M} \sum_m^M d_m^b$
and $d_{a/b}$ as in Eq. (1).

The normalized Euclidean distance D_E is the length of the line segment between the two points X_a and X_b divided by the maximal overall distance between all points:

$$D_E = \frac{\sqrt{(x_a - x_b)^2 + (y_a - y_b)^2 + (y_a - y_b)^2}}{D_{max}} \tag{6}$$

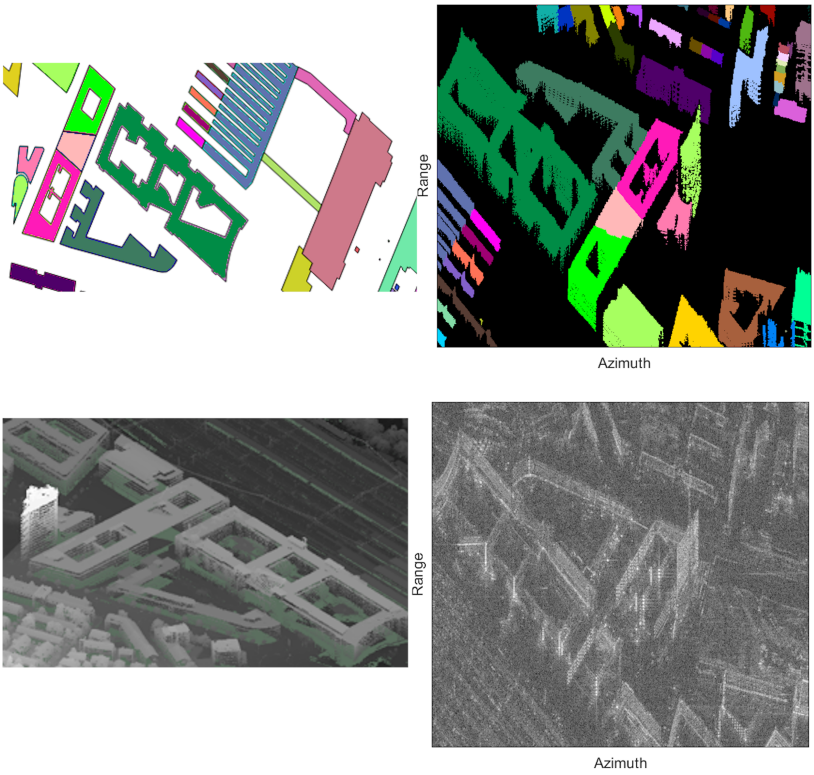

Fig. 2. Exemplary Scene and results from the Reverse Geocoding. **Top left:** OpenStreetMap labels. **Bottom left:** Digital surface model. **Top right:** SAR image in slant-range geometry. **Bottom right:** Labels in slant-range geometry.

where D_{max} is the maximal Euclidean distance between all other points, with X_a defined as in Eq. (2).

This hybrid definition of the distance groups points that show a similar deformation behavior and are not far in Euclidean space.

2.7 Uniform Manifold Approximation and Projection

As [2] have shown, dimension reduction can drastically improve the performance of a following clustering and minimizes the need of hyper parameter tuning. We are aware that such dimensionality reduction might lead to an artificial split of bigger clusters. This is acceptable trade off since we are interested in reliably finding clusters on a city wide scale and can therefore not do hyper parameter tuning for each individual building. One could tackle this issue by regrouping clusters as shown in [15], however the authors of these previous studies don't suggest a large benefit.

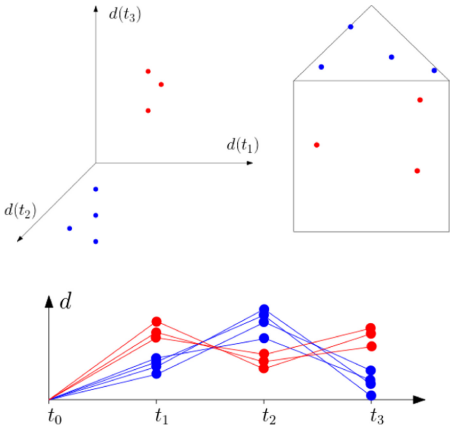

Fig. 3. Representations of PS points. **Top right**: on building. **Bottom**: deformation time series. **Top left**: in deformation space. The assumption is that points which lay on a rigid structure e.g. the roof show similar deformation behavior and therefore form clusters in deformation space.

The non-linear dimension reduction technique Uniform Manifold Approximation and Projection (UMAP) [12] is used to reduce the $(M+3)$-dimensions drastically to a two-dimensional space. We are using the distance metric D as defined in Eq. (3) to model the relationship of the PS points in $(M+3)$-dimensions.

For the UMAP hyper parameter, we use random initialization, with minimum neighbor number of 5 and a minimum distance of 0.3. We found that an iteration for 5000 epochs reliable converges towards a stable embedding.

2.8 Clustering Workflow

Each point in the embedded result is characterized by the core distance (CD) density estimator [3]. We exclude all points that have a bigger CD than twice the median overall CD. The remaining points are clustered with the density-based spatial clustering of applications with noise (DBSCAN) approach [7] with $minPts{=}5{+}\lceil\frac{N}{1000}\rceil$ (N is the total number of PS points on the building). The hyper parameter ϵ is set to the overall median of CD. Finally, we remove points from each cluster if their correlation distance D_C to the mean of the cluster is bigger than 0.3. A schematic workflow with exemplary interim results is presented in Fig. 4.

3 Experiments

To evaluate our proposed workflow, we choose a building complex that suffers known damage from underground construction activities. We can assign 185 PS points to the building. The UMAP plot with the resulting clusters are presented

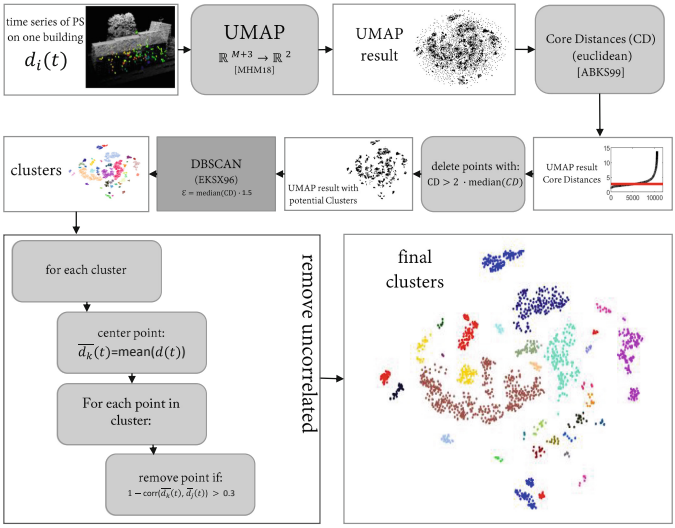

Fig. 4. Schematic workflow of the clustering process. The $(M + 3)$ dimensional PS points on a single building are embedded into a 2D space via UMAP. For all points in this embedding the core distance CD is estimated. Points that have a CD greater than twice the overall median are then excluded. DBSCAN is then performed on the remaining points (minPts $= 5$, $\varepsilon = median(CD) \cdot 1.5$). For each point in each cluster the distance to the cluster's center of gravity in the original M-dimensional deformation space is then calculated using the correlation based distance D_C. Based on this metric points are excluded from a cluster if their correlation distance is greater than a empirical threshold ($D_C = 0.3$) [15].

in Fig. 5, along with the PS points on the building and the corresponding time series. The clustering workflow shows that the deformation behavior can be grouped in several areas that follow a unique deformation behavior.

In the time series in Fig. 5, we can observe a relief rupture (Fig. 6) in May 2019, that coincides with press reports about compression injections due to an ongoing tunnel project under this area [17]. The time series also indicate a stabilization of these structures over the period of the following year.

We also investigated a much larger building in the same data set. The resulting 69 clusters along with their time series are presented in the supplementary material (see Appendix in Sect. 5). Here we can observe the annual temperature oscillation along with post-construction subsidence in the order of several millimeters per year.

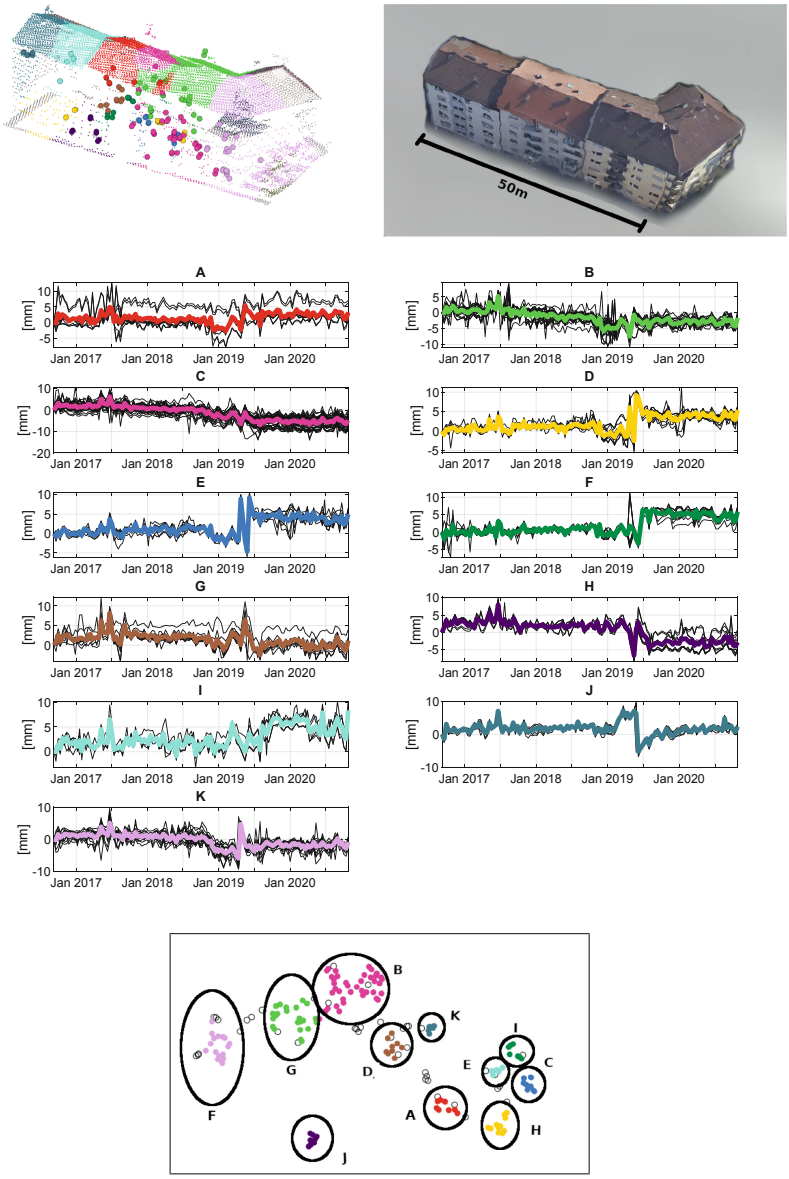

Fig. 5. Left: First from the top: Spatial distribution of 144 PS points on a small urban building complex, super imposed with an ALS-point cloud. The colors indicate the membership to the extracted clusters. **Second from the top**: textured mesh representation of the same building complex. **The time series A to K** show the deformation behavior for each of the extracted cluster. The bold, colored graph represents the centroid of the cluster in deformation space as defined in Fig. 3. **Bottom**: UMAP's low-dimensional embedding of all PS points. The color and letter correspond with the time series and spatial distribution above. Points that were excluded during the clustering process (see Sect. 2.8) are drawn in white.

Fig. 6. Cracks in the building started to appear at the same time (May 2019) as the observed release rupture in the time series (Fig. 5).

4 Conclusions and Future Work

We propose a new distance metric to describe the similarity of persistent scatterers on single buildings. The metric considers the similarity of the deformation histories and the spatial distance of the points. This allows to group the PS points into clusters that show an equal deformation behavior but does suppress groups of points that are distributed too far on the building. Our experiments show that this metric combined with a dimension reduction and clustering approach can reliably extract plausible groups of PS points that are locally connected and show the same deformation behavior over time. The visualization of those clusters, their spatial distribution and the related time series is exemplary shown in a web-based tool, that allows decision makers an insight into deformation events, beyond the traditional two dimensional superposition with an orthophoto.

Further experiments need to include more semantic information of the buildings to link the extracted clusters to specific structures. This allows an integration of the persistent scatterer interferometry technique into building information modeling systems. Another long term aim of this work is an automated city-wide monitoring approach. By extracting clusters and analyzing the deformation patterns relative to each other, structural stress could be observed. This could lead to a per-building risk and damage assignment.

Acknowledgements. The SAR data were provided by the *German Aerospace Center* (DLR) through the proposal LAN0634. We would like to thank the *State Office for Spatial Information and Land Development Baden-Württemberg* (LGL) for providing citywide ALS/Mesh data and orthophotos.

5 Appendix

As supplementary material, we provide an online visualization of the above presented results. We also provide a secondary, much larger building from the same

data set. Those visualizations allow an three-dimensional investigation of the achieved results. A colorized ALS point cloud is shown together with the PS points. The clusters are color coded and correspond with the extracted time series on the right hand side.

Building 1: https://ifpwww.ifp.uni-stuttgart.de/philipp/gcpr2021/building1/
Building 2: https://ifpwww.ifp.uni-stuttgart.de/philipp/gcpr2021/building2/

References

1. Airbus: TerraSAR-X Image Product Guide - Basic and Enhanced Radar Satellite Imagery, February 2020. https://www.intelligence-airbusds.com/files/pmedia/public/r459_9_20171004_tsxx-airbusds-ma-0009_tsx-productguide_i2.01.pdf, October 2017, https://www.intelligence-airbusds.com/files/pmedia/public/r459_9_20171004_tsxx-airbusds-ma-0009_tsx-productguide_i2.01.pdf
2. Allaoui, M., Kherfi, M.L., Cheriet, A.: Considerably improving clustering algorithms using UMAP dimensionality reduction technique: a comparative study. In: El Moataz, A., Mammass, D., Mansouri, A., Nouboud, F. (eds.) ICISP 2020. LNCS, vol. 12119, pp. 317–325. Springer, Cham (2020). https://doi.org/10.1007/978-3-030-51935-3_34
3. Ankerst, M., Breunig, M.M., Kriegel, H.P., Sander, J.: Optics. ACM SIGMOD Rec. **28**(2), 49–60 (1999). https://doi.org/10.1145/304181.304187
4. Costantini, M., et al.: Automatic detection of building and infrastructure instabilities by spatial and temporal analysis of insar measurements. In: IGARSS 2018–2018 IEEE International Geoscience and Remote Sensing Symposium, pp. 2224–2227 (2018)
5. Crosetto, M., Monserrat, O., Cuevas-González, M., Devanthéry, N., Luzi, G., Crippa, B.: Measuring thermal expansion using X-band Persistent Scatterer Interferometry. ISPRS J. Photogramm. Remote. Sens. **100**, 84–91 (2015)
6. Crosetto, M., Monserrat, O., Cuevas-González, M., Devanthéry, N., Crippa, B.: Persistent scatterer interferometry: a review. ISPRS J. Photogramm. Remote Sens. **115**, 78–89 (2016). https://doi.org/10.1016/j.isprsjprs.2015.10.011
7. Ester, M., Kriegel, H.P., Sander, J., Xu, X.: A density-based algorithm for discovering clusters in large spatial databases with noise. In: Proceedings of the Second International Conference on Knowledge Discovery and Data Mining. KDD 1996, pp. 226–231. AAAI Press (1996). http://dl.acm.org/citation.cfm?id=3001460.3001507
8. Ferretti, A., Prati, C., Rocca, F.: Permanent scatterers in SAR interferometry. IEEE Trans. Geosci. Remote Sens. **39**(1), 8–20 (2001). https://doi.org/10.1109/36.898661
9. Ferretti, A., Prati, C., Rocca, F.: Nonlinear subsidence rate estimation using permanent scatterers in differential SAR interferometry. IEEE Trans. Geosci. Remote Sens. **38**, 2202–2212 (2000). https://doi.org/10.1109/36.868878
10. Gernhardt, S., Adam, N., Eineder, M., Bamler, R.: Potential of very high resolution SAR for persistent scatterer interferometry in urban areas. Ann. GIS **16**, 103–111 (2010)
11. Maccabiani, J., Nicodemo, G., Peduto, D., Ferlisi, S.: Investigating building settlements via very high resolution SAR sensors. In: Proceedings of the Fifth International Symposium on Life-Cycle Civil Engineering. IALCCE 2016, p. 8, January 2017. https://doi.org/10.1201/9781315375175-332

12. McInnes, L., Healy, J., Saul, N., Großberger, L.: UMAP: uniform manifold approximation and projection. J. Open Source Softw. **3**(29), 861 (2018). https://doi.org/10.21105/joss.00861
13. SARMAP: Sarscape: Technical description. SARMAP: Purasca, May 2020. http://www.sarmap.ch/tutorials/PS_v553.pdf
14. Schneider, P.J., Khamis, R., Soergel, U.: Extracting and evaluating clusters in dinsar deformation data on single buildings. ISPRS Ann. Photogramm. Remote Sens. Spat. Inf. Sci. **V-3-2020**, 157–163 (2020). https://doi.org/10.5194/isprs-annals-v-3-2020-157-2020
15. Schneider, P.J., Soergel, U.: Segmentation of buildings based on high resolution persistent scatterer point clouds. ISPRS Ann. Photogramm. Remote Sens. Spat. Inf. Sci. **V-3-2021**, 65–71 (2021). https://doi.org/10.5194/isprs-annals-V-3-2021-65-2021, https://www.isprs-ann-photogramm-remote-sens-spatial-inf-sci.net/V-3-2021/65/2021/
16. Schunert, A., Schack, L., Soergel, U.: Matching persistent scatterers to buildings. ISPRS - Int. Arch. Photogramm. Remote Sens. Spat. Inf. Sci. **XXXIX-B7**, 79–84 (2012). https://doi.org/10.5194/isprsarchives-xxxix-b7-79-2012
17. SWR: Risse in Hauswänden - verursacht durch Stuttgart 21. [YouTube video], May 2019. https://www.youtube.com/watch?v=CawL7bCnNpg. Accessed 25 May 2021
18. Tanaka, T., Hoshuyama, O.: Persistent scatterer clustering for structure displacement analysis based on phase correlation network. In: 2017 IEEE International Geoscience and Remote Sensing Symposium (IGARSS). IEEE, July 2017. https://doi.org/10.1109/igarss.2017.8128030
19. Yang, C.H.: Spatiotemporal change detection based on persistent scatterer interferometry: a case study of monitoring urban area (2019). https://doi.org/10.18419/OPUS-10423
20. Zhu, M., et al.: Detection of building and infrastructure instabilities by automatic spatiotemporal analysis of satellite SAR interferometry measurements. Remote Sens. **10**(11), 1816 (2018). https://doi.org/10.3390/rs10111816